The effect of chemistry and thermal fluctuations on charge injection barriers at aluminum/polyolefin interfaces

Yiyuan Wang ✉ 🄳 ; Sari J. Laihonen 🄳 ; Mikael Unge 🄳 ; Arash A. Mostofi 🄳

Check for updates

CrossMark

View Online

Export Citation

Articles You May Be Interested In

Challenges in Materials Transformation Modeling for Polyolefins Industry

AIP Conference Proceedings (June 2004)

Modified talcum as crosslinking agent for polyolefins

AIP Conference Proceedings (August 2019)

Crosslinked polyolefins using a modified filler

AIP Conference Proceedings (February 2019)

AIP Publishing

The effect of chemistry and thermal fluctuations on charge injection barriers at aluminum/polyolefin interfaces

View Online   Export Citation   CrossMark

Yiyuan Wang,[1,a)] Sari J. Laihonen,[2] Mikael Unge,[3] and Arash A. Mostofi[1,b)]

AFFILIATIONS

[1]Departments of Materials and Physics and the Thomas Young Centre for Theory and Simulation of Materials, Imperial College London, Exhibition Road, London SW7 2AZ, United Kingdom
[2]Hitachi Energy Research, Forskargränd 7, 721 78 Västerås, Sweden
[3]NKT HV Cables AB, Technology Consulting, 722 26 Västerås, Sweden

[a)]Author to whom correspondence should be addressed: amyyiyuan627@gmail.com
[b)]Email: a.mostofi@imperial.ac.uk

ABSTRACT

Charge injection at metal/polymer interfaces is a critical process in many technological devices, including high voltage capacitors and cables in which polyolefin materials, such as polyethylene (PE) and polypropylene (PP), are often used as insulation materials. We use simulations based on density-functional theory to study charge injection at aluminum/PE and aluminum/PP interfaces. Specifically, we investigate the influence of incorporating a variety of polar chemical impurities at the PE and PP chain ends on electron and hole injection barriers. Crucially, we account for the effect of thermal disorder by considering ensembles of thousands of interface structures obtained from *ab initio* molecular dynamics trajectories at 373 K. We show that the mean injection barrier can change by up to 1.1 eV for Al/PE and 0.6 eV for Al/PP, as compared to the pristine case, depending on which chemical impurity is introduced. We also show that the spread of injection barriers from thermal fluctuations also depends strongly on the chemistry of the impurity. The observed trends can be understood with a simple model based on thermal fluctuations of the dipole moment density associated with the chemical impurity at the interface. We further verify this model by considering larger interface models with lower impurity densities. Our results demonstrate that small chemical modifications, which may arise from oxidation, for example, have a significant influence on charge injection barriers in metal/polyolefin interfaces.

I. INTRODUCTION

Charge injection at metal/polymer interfaces is an important phenomenon in technological applications, such as polymer electronic devices (e.g., organic light emitting diodes and organic solar cells) and high voltage equipment (e.g., cables, capacitors, and transformers). For high voltage applications, where polyolefins, such as polyethylene (PE)[1,2] and polypropylene (PP),[3,4] are typically used to insulate metallic conductors in cables and capacitors, respectively, it is important to minimize charge injection at the metal/polyolefin interface and, hence, leakage current to avoid unnecessary energy loss from the conductor and degradation and eventual failure of the insulator.[5,6]

To achieve this goal, it is desirable to understand how charge injection barriers are influenced by the atomic structure of the interface, including the type and surface orientation of the metal electrode and polyolefin insulator; the extent of oxidation of the metal surface and its microstructure; the degree of crystallinity of the polyolefin, which will usually contain a mixture of crystalline and amorphous regions with a distribution of local disorder, such as kinks and branches in the polymer chains;[7] and the presence of chemical defects, such as unsaturated bonds and oxygen-containing groups[8] as well as additives[9] and reaction by-products.[10]

For example, in high voltage metallized film capacitors, the insulation material, typically a biaxially oriented polypropylene

(BOPP) film, and the metal electrode, are integrated together; i.e., the electrode is evaporated directly on the BOPP film. To improve the adhesion between the BOPP film and the metal, air or oxygen plasma treatment[11–13] can be performed on the BOPP film surface to introduce oxygen-containing polar groups, such as hydroxyl OH, carbonyl C=O, carboxylic acid O=C–OH and ester O=C–O to the BOPP film surface. Halogen groups, such as –F, –Cl, and –Br, can also be introduced to polyolefin surfaces with plasma treatment.[14] While this process aids the adhesion of the interface, the mechanism of its influence on charge injection is not well understood.[6]

Experimentally, it is challenging to understand the individual effects of these factors on charge injection barriers. In terms of theoretical research, macroscopic transport models[15] have been developed to understand elementary processes, such as charge injection and charge transport within polyolefins sandwiched between metal electrodes. Such models have been used to study the effects of interface trap states[16] and interface roughness[17,18] on charge injection at metal/polyolefin interfaces. The parameters used in such models, however, are usually obtained by fitting the results to experimental data, such as inferred space charge profiles and leakage currents. A crucial limitation is that they cannot predict how changes at the atomic or molecular level at metal/polyolefin interfaces give rise to changes in charge injection barriers. In contrast, first-principles electronic structure simulations, such as those based on density functional theory (DFT), do not require any external parameterization and have the potential to qualitatively and quantitatively predict how charge injection barriers are influenced by changes in atomic and molecular structures at metal/polyolefin interfaces.[7,19–21] For example, in Ref. 19, charge injection barriers were calculated for idealized model interfaces with different metal (111) surfaces (namely, Al, Ag, Cu, Pd, and Pt) and different orientations of PE, including with PE chains parallel and perpendicular to the interface plane. A key conclusion of this study was that the structure and bonding at the interface have a crucial role in determining the charge injection barrier.

In this work, we use DFT calculations to study charge injection barriers at Al/PE and Al/PP interfaces. In particular, we focus on four different polar chemical groups, namely, –COOH, –OH, –CHO, and –Cl, that are incorporated at the interface. These chemical impurities are placed at the terminating ends of the PE and PP oligomers at the interface. We choose aluminum (Al) for the metal electrode as it is commonly used in high voltage power applications.[1,3] We use idealized interface models in which both Al electrodes and polyolefin insulators are prepared in a commensurate crystalline structure. We then use *ab initio* molecular dynamics (AIMD) simulations at a temperature of around 373 K, which is approximately the maximum practical working temperature of PE and PP,[22,23] to study the effect of thermal disorder on charge injection barriers. We take ensembles of snapshots of the interface structures from long AIMD simulations to obtain distributions of charge injection barriers that arise from thermal fluctuations.

For both Al/PE and Al/PP interfaces, we find that incorporating –COOH, –OH, –CHO, or –Cl chemical impurities at the interface strongly affects the distribution of charge injection barriers that is induced by thermal fluctuations. For all of the chemical impurities studied, the spread of charge injection barriers is much

larger than in the pristine case, with the widest spread resulting from –OH and the narrowest from –Cl. The mean of the charge injection barrier distribution varies by up to 1.1 eV for Al/PE and 0.6 eV for Al/PP depending on which chemical impurity is present. We show that these results can be understood using a simple model that is based on the magnitude of the dipole moment density associated with the chemical impurity at the interface and the orientations it explores as a result of thermal fluctuations. The model is further verified by considering different surface densities of chemical impurities at the interface. This work demonstrates that oxidation at the interface, resulting from plasma treatment, for example, can result in charge injection barriers that are quite different from the pristine case and can, therefore, influence the performance of the system.

The remainder of the paper is organized as follows. In Sec. II, we describe our method for calculating charge injection barriers at Al/polyolefin interfaces, as well as details of our atomistic models and AIMD simulations. We also present benchmark results for bulk Al, PE, and PP and provide the parameters used in all our calculations. In Sec. III, we present and discuss our results for Al/PE and Al/PE interfaces with and without chemical impurity groups at the interface. In Sec. IV, we summarize the main conclusions of our work.

II. METHODS

A. Bulk-reference method

We calculate charge injection barriers at Al/PE and Al/PP interfaces using the so-called bulk-reference method.[24,25] We use an Al/PE interface as an example to illustrate the approach, as shown in Fig. 1. The simulation cell consists of a slab of Al
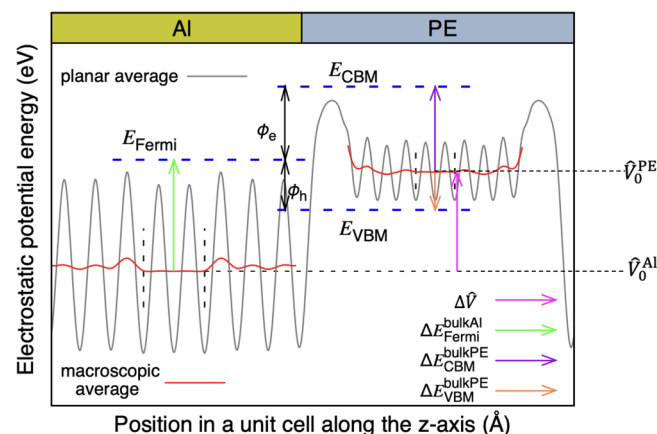

FIG. 1. The band alignment at an Al/PE interface within the "bulk-reference" method. The regions between two black dashed lines of Al and PE show the "bulk-like" regions away from the interface. E_{Fermi}, E_{CBM}, and E_{VBM} are the Al Fermi level and the PE conduction band minimum (CBM) and the PE valence band maximum (VBM), respectively, in the bulk-like regions. $\hat{V}_0^{Al}$ and $\hat{V}_0^{PE}$ are the values of $\hat{V}(z)$ in the bulk-like region of the interface system on the Al and PE side of the interface, respectively, and $\Delta\hat{V}$ is the macroscopic average potential difference across the interface. ϕ_e and ϕ_h are electron and hole injection barriers, respectively, defined in Eqs. (6) and (7).

interfaced with a slab of PE, with periodic boundary conditions along all three axes. We define the direction perpendicular to the interface plane to be the z axis. For the particular case shown in Fig. 1, along the z axis, the simulation cell consists of nine atomic layers of Al interfaced with PE oligomers that have nine carbon atoms along their backbone.

With reference to Fig. 1, the electron ϕ_e and hole ϕ_h injection barriers at an Al/PE interface are defined as

$$\phi_e = E_{CBM} - E_{Fermi}, \quad (1)$$

$$\phi_h = E_{Fermi} - E_{VBM}, \quad (2)$$

where E_{Fermi}, E_{CBM}, and E_{VBM} are defined as the Fermi level in Al, and the conduction band minimum (CBM) and the valence band maximum (VBM) in PE, in regions far away from the interface that are considered to be "bulk-like." These bulk-like regions are taken to be the central part of the Al and PE slabs that make the interface simulation cell, denoted by the vertical dashed black lines in Fig. 1. The figure also shows the planar average electrostatic potential $\overline{V}(z)$ (gray line) and the macroscopic average potential $\widehat{V}(z)$ (red lines). $\overline{V}(z)$ is calculated by averaging the electrostatic potential over the directions parallel to the interface plane; $\widehat{V}(z)$ is obtained by convolving $\overline{V}(z)$ at each side of the interface region with a rectangular filter function whose width is the interlayer spacing of that side. For each side, it can be seen that $\widehat{V}(z)$ is flat in the bulk-like region.

In the "bulk-reference" approach,[24,25] E_{Fermi}, E_{CBM}, and E_{VBM} are calculated by referencing them to $\widehat{V}(z)$ in the bulk-like regions of the interface system using the relative positions of the same quantities in bulk Al and PE, which are obtained from separate DFT calculations on bulk Al and bulk PE. Mathematically,

$$E_{Fermi} = \widehat{V}_0^{Al} + \underbrace{E_{Fermi}^{bulkAl} - \widehat{V}^{bulkAl}}_{\Delta E_{Fermi}^{bulkAl}}, \quad (3)$$

$$E_{CBM} = \widehat{V}_0^{PE} + \underbrace{E_{CBM}^{bulkPE} - \widehat{V}^{bulkPE}}_{\Delta E_{CBM}^{bulkPE}}, \quad (4)$$

$$E_{VBM} = \widehat{V}_0^{PE} + \underbrace{E_{VBM}^{bulkPE} - \widehat{V}^{bulkPE}}_{\Delta E_{VBM}^{bulkPE}}, \quad (5)$$

where $\widehat{V}_0^{Al}$ and $\widehat{V}_0^{PE}$ are the values of $\widehat{V}(z)$ in the bulk-like region of the interface system on the Al and PE side of the interface, respectively (as indicated by the horizontal black dashed lines in Fig. 1), and the terms that are underbraced, namely, $\Delta E_{Fermi}^{bulkAl}$, ΔE_{CBM}^{bulkPE}, and ΔE_{VBM}^{bulkPE}, are obtained from separate calculations on bulk Al and bulk PE and are the bulk referencing shifts (schematically shown by the green, purple, and orange arrows in Fig. 1). As indicated by the underbraces in Eqs. (3)–(5), these bulk-referencing shifts are given by, respectively, the position of the Fermi level of bulk Al, denoted E_{Fermi}^{bulkAl}, relative to the macroscopic average potential in bulk Al, denoted $\widehat{V}^{bulkAl}$; and the position of the CBM (VBM) in

bulk PE, denoted E_{CBM}^{bulkPE} (E_{VBM}^{bulkPE}), relative to the macroscopic average potential in bulk PE, denoted $\widehat{V}^{bulkPE}$.

Substituting Eqs. (3)–(5) into Eqs. (1) and (2), we obtain

$$\phi_e = \Delta \widehat{V} + \Delta E_{CBM}^{bulkPE} - \Delta E_{Fermi}^{bulkAl}, \quad (6)$$

$$\phi_h = \Delta E_{Fermi}^{bulkAl} - \Delta \widehat{V} - \Delta E_{VBM}^{bulkPE}, \quad (7)$$

where we have defined $\Delta \widehat{V}$ as the macroscopic average potential difference across the interface,

$$\Delta \widehat{V} = \widehat{V}_0^{PE} - \widehat{V}_0^{Al}. \quad (8)$$

From Eqs. (6) and (7), it is clearly seen that the sum of ϕ_e and ϕ_h is the band gap of bulk PE.

B. Bulk systems

The PWscf code of the Quantum ESPRESSO software package[26] was used to carry out all DFT calculations reported in this work.

For bulk Al, we used the PBE generalized gradient approximation functional[27] to describe exchange and correlation effects and a norm-conserving pseudopotential of the RRKJ type[28] to describe the combined effect of screened potential due to the nucleus and core electrons. The kinetic energy cutoff for the plane-wave expansion of the electronic wave functions was 32 Ry and that for charge density was 128 Ry. To obtain the equilibrium lattice constant, the Brillouin zone was sampled with a Monkhorst–Pack mesh of $8 \times 8 \times 8$ k-points. To obtain the Fermi level, a $24 \times 24 \times 24$ k-point mesh was used. The "Marzari–Vanderbilt" smearing method was used with a smearing width of 0.01 Ry. The calculated equilibrium lattice constant a_0 of a FCC unit cell of Al was 4.06 Å, which agrees well with the experimental value of 4.05 Å.[29]

The crystal structures of bulk PE and PP have an orthorhombic and monoclinic unit cells, respectively. Structural relaxations were performed using the vdW-DF[30–33] functional for exchange and correlation, which accounts for non-local van der Waals interactions that are an important component of the inter-chain binding energy in these systems. Ultrasoft pseudopotentials of the RRKJ type[28] were used for C and H. The kinetic energy cutoffs for wave functions (charge density) were 64 (256) and 48 Ry (192 Ry), respectively, and the Monkhorst–Pack meshes for sampling the Brillouin zone were $2 \times 4 \times 8$ and $3 \times 1 \times 3$, respectively. For geometry optimization, the force and energy convergence thresholds for PE were 2.6×10^{-3} eV/Å and 1.36×10^{-6} eV, respectively, and for PP, they were 2.6×10^{-2} eV/Å and 1.36×10^{-3} eV, respectively. The calculated equilibrium lattice constants are summarized in Table I, which are in good agreement with experimental measurements.[34,35] For PP, β is the angle between lattice vectors **a** and **c**.

It is well known that DFT exchange and correlation functionals, such as those based on the local density or generalized gradient approximation (including van der Waals functionals based on them), do not predict electronic bandgaps and, hence, the position of valence and conduction band edges, accurately; for example, we calculate the bandgaps of bulk PE and PP with the vdW-DF

TABLE I. Bulk PE and PP equilibrium lattice constants.

Polyolefin	Method	a (Å)	b (Å)	c (Å)	β
PE	Calculated	7.31	5.17	2.57	
	Experiment[34]	7.12	4.85	2.55	
PP	Calculated	6.76	20.49	6.59	98.5°
	Experiment[35]	6.65	20.96	6.50	99.2°

functional to be 6.38 and 6.13 eV, respectively, which are much lower than the experimental values of 8.8[36] and 8.4 eV.[37] For this reason, we use the PBE0[38] hybrid exchange and correlation functional for computing the band edge positions in our relaxed bulk PE and PP structures. The calculated bandgaps for PE and PP are 8.42 and 8.26 eV, respectively. Compared to the vdW-DF, with PBE0, the VBM of PE (PP) is shifted downward by 1.10 eV (1.11 eV) and the CBM of PE (PP) is shifted upward by 0.94 eV (1.02 eV), which is in good agreement with previous hybrid functional calculations on PE.[19,39]

C. Interface systems

In this work, we have studied Al(100)/PE(001) and Al(100)/PP(001) interfaces. The pristine interface supercells are shown in Figs. 2(a) and 2(b), respectively. In the direction perpendicular to the interface, we used 9 atomic layers of Al together with PE (PP) oligomers with 9 (12) carbon atoms along their backbone for Al/PE (Al/PP) to limit the interaction between periodically repeated interfaces. To lattice match Al and PE (PP) in the interface plane, we used the equilibrium lattice constant of Al and imposed strain on PE (PP). For Al/PE, a $2a_0 \times 1a_0$ Al(100) surface unit cell was matched with a $1a \times 1b$ PE(001) surface unit cell, and for Al/PP, a $\sqrt{10}a_0/2 \times 3\sqrt{10}a_0/2$ Al(100) surface unit cell was matched with a $1a \times 1b$ PP(001) surface unit cell, where a_0 and a (along the x-axis) and b (along the y-axis) are the calculated equilibrium lattice constants for bulk Al and bulk PE (or PP), respectively. The required strains in the x and y-directions on PE (PP) were 11% (5%) and 22% (6%), respectively. The numbers of atoms in the Al/PE and Al/PP simulation cells are 94 and 359, respectively. The separation distance between the Al and PE (or PP) regions was varied, and, in each case, the atomic positions were relaxed. In this way, the lowest energy structure with optimized separation and atomic structure was determined.

For computing the electronic properties of bulk PE and PP needed in the bulk-reference method, bulk calculations were performed on bulk PE and PP structures with the same mismatch strain imposed as in the interface systems. The bandgaps of bulk PE and PP under the interface mismatch strain were calculated with PBE0 to be 8.16 and 7.89 eV, respectively.

The four chemical groups studied in this work are shown in Fig. 2(c). They were incorporated at the PE and PP chain ends, marked within red dashed boxes in Figs. 2(a) and 2(b). Initially, we considered Al/PE (Al/PP) interfaces with one modified PE (PP) chain for every two (four) chains in the interface simulation cell, which we denote as a "1/2" ("1/4") surface density of chemical modifiers. We note that for Al/PE, the two interfaces present in the

(a)

(b)

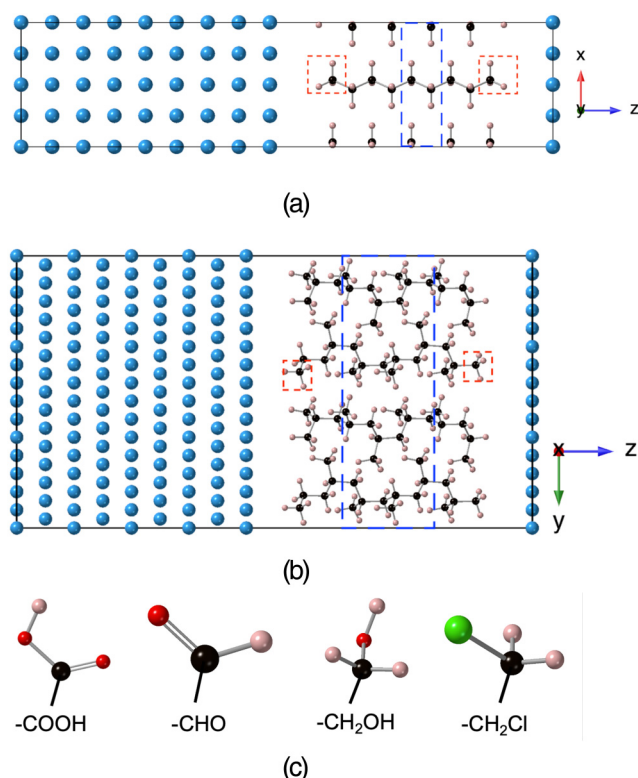-COOH   -CHO   -CH₂OH   -CH₂Cl

(c)

FIG. 2. (a) Pristine Al(100)/PE(001) interface simulation cell (periodic boundary conditions apply in all three Cartesian directions). A primitive unit cell of PE is indicated by the blue dashed line. The conventional crystal axes of Al and PE are aligned with the x, y, and z axes of the periodic simulation cell. (b) Pristine Al(100)/PP(001) simulation cell (periodic boundary conditions apply in all three Cartesian directions). A primitive unit cell of PP is indicated by the blue dashed line. The orientation of the interface is such that the [100] and [010] crystal axes of PP are aligned with the x and y axes of the simulation cell, while the [001] crystal axis is at an angle of 8.5° with respect to the z axis of the simulation cell, while for Al, the [100] direction of the conventional unit cell is aligned with the z axis of the simulation cell, and the [010] and [001] directions are rotated by 18.43° with respect to the x and y axes of the simulation cell. (c) Four chemical groups that are introduced at the interface. The colors for Al, C, H, O, and Cl are blue, black, pink, red, and green, respectively. The red dashed lines in (a) and (b) mark regions where these chemical groups are substituted.

simulation cell were constructed to be symmetric about the center of the PE slab, whereas for Al/PP, due to the lack of a mirror plane parallel to the interface of the bulk PP unit cell, an equivalent symmetric construction is not possible. The separation of the Al and PE (or PP) regions and equilibrium atomic structures for the chemically modified interface systems were determined in a similar manner to the approach described earlier for pristine interfaces.

In all calculations on Al/PE and Al/PP interfaces, we used the vdW-DF exchange and correlation functional. For Al/PE and Al/PP, the kinetic energy cutoffs for wave functions (charge density) were 64 (256) and 48 Ry (192 Ry), respectively. The force and total energy convergence thresholds for Al/PE (Al/PP)

interfaces were 1.3×10^{-2} eV/Å (1.0×10^{-2} eV/Å) and 1.36×10^{-4} eV (1.0×10^{-3} eV), respectively. The atomic positions of the middle three Al and PE unit cells and the middle PP unit cell in each half of the interface system were fixed to ensure that these regions in the interior of the slabs remain bulk-like.

D. *Ab initio* molecular dynamics simulations

Starting from the optimized interface structures described above, we performed AIMD simulations to obtain trajectories of Al/PE and Al/PP interface atomic conformations. In practice, the maximum continuous working temperature of cross-linked polyethylene in HVDC cables is around 90°C,[22] and the maximum operating temperature of PP capacitors is 105°C.[23] Therefore, the target temperature in all AIMD simulations was set to be 373 K (100°C), which is close to the working temperature of both PE and PP. We used an NVT ensemble with a velocity rescaling thermostat and a time step of 0.5 fs. Once the temperature converged to within 15 K of the target temperature of 373 K, snapshots were taken every 5 fs until a total of 500 snapshots had been collected (i.e., a production run of 2.5 ps).

E. Dipole moments of chemical modifiers

During an AIMD simulation, the chemical modifiers introduced at the interface undergo thermal fluctuations and, in particular, explore a range of orientations. As we discuss later, this turns out to be an important factor in understanding the electrical properties of the interface. For this reason, for each AIMD snapshot, we calculated the dipole moment associated with the chemical modifier at each interface by extracting it from the structure and treating it as a molecule whose dipole moment we then computed. In more detail, we cut at the C–C bond immediately adjacent to the chemical group and passivated it with a hydrogen atom. The resulting molecule was then isolated in a $10 \times 10 \times 10 \, \text{Å}^3$ simulation cell and its dipole moment is calculated. The calculated dipole of this molecule should be very close to the dipole of the corresponding chemical group in the full interface because the C–C bond and the C–H bond are non-polar or almost non-polar. Since the charge injection process is across the interface, i.e., along the z axis, the z-component of the dipole moment D_z is our primary focus. We also define the z-component of the dipole moment surface density ρ_{D_z} at an Al/PE or Al/PP interface as

$$\rho_{D_z} = D_z/A, \qquad (9)$$

where A is the area of Al/PE or Al/PP interfaces in the simulation cell.

F. Symmetrization of interface snapshots

For Al/PE snapshots, the initial mirror symmetry of the two Al/PE interfaces in each simulation is broken by thermal fluctuations during the AIMD simulations. Since this usually results in an overall electrostatic dipole across the system, the calculated macroscopic average potential for an asymmetric interface configuration usually shows a slope in the interior atomic region of each material, making it difficult to determine precisely the value of $\hat{V}_0^{PE}$ and $\hat{V}_0^{Al}$

in charge injection barrier calculations. To circumvent this, we use each snapshot to construct two distinct symmetrized interface simulation cells by applying mirror symmetry to one or other of the two interfaces in the original snapshot. In this way, for each chemistry, 1000 symmetrized Al/PE snapshots are obtained from the 500 AIMD snapshots, and charge injection barriers were computed for these symmetrized simulation cells.

For Al/PP, as noted earlier, neither the initial structure nor the AIMD snapshots have mirror symmetry. For each chemistry, 500 pairs of individual interface configurations were chosen from the total of 1000 interface configurations that were present in the original 500 AIMD snapshots. These pairs were then combined to construct 500 unique interface simulation cells, which we refer to as "composite" Al/PP snapshots, and charge injection barriers were computed for these composite simulation cells. Our criterion for matching up pairs of interfaces was that the associated chemical modifiers have a dipole moment D_z differing by no more than 0.01 eÅ, so as to minimize any overall dipole moment across the system that results from asymmetry of the two interface regions in each composite snapshot.

For the DFT calculations on the large set of several thousand AIMD simulation cells described above, the Monkhorst–Pack meshes for sampling the Brillouin zone were $2 \times 4 \times 1$ and $3 \times 1 \times 1$ for symmetrized Al/PE snapshots and composite Al/PP snapshots, respectively.

III. RESULTS AND DISCUSSION

For Al/PE (Al/PP), we calculated the distribution of charge injection barriers resulting from thermal fluctuations for the 1000 (500) symmetrized (composite) snapshots for each interface chemistry, and the results are shown in Fig. 3(a) [Fig. 3(b)]. The horizontal axis shows the number of conformations, and the left and right vertical axes show the electron (ϕ_e) and hole (ϕ_h) injection barriers, respectively. The mean charge injection barrier of each distribution is denoted by the central red data point in each panel, with the mean ϕ_e and ϕ_h displayed to the left and right of it, respectively. As is immediately apparent from these distributions, the mean charge injection barrier for Al/PE (Al/PP) can be changed by up to 1.1 eV (0.6 eV) with different chemical modifiers. For pristine Al/PE interfaces (denoted as –CH$_3$), the mean ϕ_e is 4.62 eV, which is 1.1 eV higher than the mean ϕ_h, suggesting that hole injection is dominant. This is qualitatively consistent with previous calculations on Al/PE interfaces.[19] For the pristine Al/PP interfaces, the mean ϕ_e and ϕ_h are similar, at around 3.9 eV.

For interfaces with chemical modifiers, the general trend for both Al/PE and Al/PP is to reduce the mean ϕ_e as compared to the pristine case and for the mean ϕ_e to become smaller than the mean ϕ_h (i.e., favoring electron injection). The exception to these trends is Al/PE interfaces with –COOH, which have similar mean ϕ_e and ϕ_h to the pristine case. The horizontal black dashed line denotes the condition for $\phi_e = \phi_h$, in other words, when the injection barrier for either electrons and holes is maximal. For Al/PE, interfaces with –CH$_2$OH show the smallest difference between the mean ϕ_e and ϕ_h at around 0.5 eV; however, they also have the widest spread in injection barriers as a result of thermal fluctuations. For interfaces with –CHO, the difference between the mean
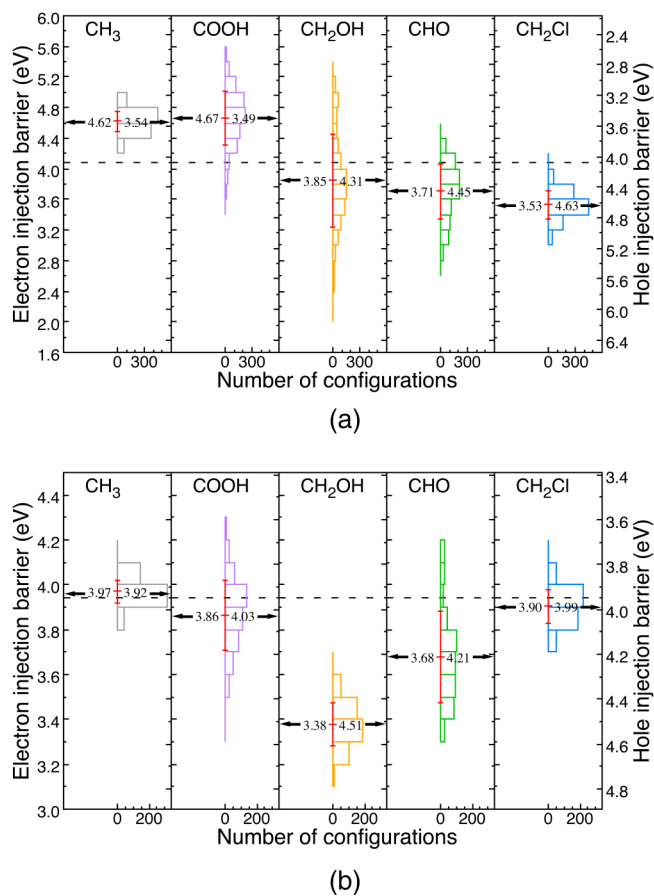
(a)

(b)

FIG. 3. Charge injection barrier distributions resulting from thermal fluctuations around 373 K for (a) Al/PE interfaces and (b) Al/PP interfaces. The pristine case (without chemical modifiers) is denoted as –CH₃. For the systems with chemical modifiers, the surface densities of chemical groups are "1/2" for Al/PE and "1/4" for Al/PP (for details, see Sec. II). In each panel, the mean charge injection barrier is shown as a red data point with the mean electron ϕ_e and hole ϕ_h injection barriers displayed to the left and right of it, respectively. The standard deviation σ_{IB} of all the injection barriers for each group is shown with the error bars above and below the red data point. The black dashed line corresponds to $\phi_e = \phi_h$. (a) Al/PE interface. (b) Al/PP interface.

ϕ_e and ϕ_h is only 0.7 eV and exhibits a moderate spread in injection barriers. For Al/PP, interfaces with –CH₂Cl have both the smallest difference between mean ϕ_e and ϕ_h and the smallest spread of injection barriers, suggesting that –CH₂Cl could be the most suitable chemical modifier for suppressing charge injection of both holes and electrons simultaneously.

Charge injection barriers cannot be directly measured experimentally, but they are often inferred from fitting macroscopic charge transport models to experimental measurements of, e.g., space charge distributions.[40] As noted by others,[7,19] such experimentally inferred injection barriers are found to be around 1 eV,[40] which is much lower than theoretically calculated barriers for pristine interfaces, shown in the left panels of Figs. 3(a) and 3(b). They

are, however, more comparable to some of our configurations with chemical modifications at the interface, for example, as shown by the large spread of injection barriers for –CH₂OH modifiers in the middle panel of Fig. 3(a).

The standard deviation σ_{IB} of the thermal distributions of charge injection barriers in Fig. 3 is denoted by the red error bars in each panel. For Al/PE (Al/PP), the pristine interfaces and the interfaces with –CH₂Cl modifiers have the smallest σ_{IB}, 0.14 (0.05) and 0.18 eV (0.08 eV). Interfaces with –COOH and –CHO have larger σ_{IB}, 0.35 (0.16) and 0.35 eV (0.20 eV), respectively. For Al/PE, interfaces with –CH₂OH have the largest σ_{IB} at 0.61 eV, while for Al/PP, it is –CHO at 0.20 eV. Overall, it can be seen that Al/PP interfaces exhibit smaller thermal variations in injection barriers than Al/PE interfaces.

We hypothesize that the distribution of injection barriers is related to the diversity of interface conformations that each chemical modifier at the interface explores during the AIMD simulations. Since the chemical modifiers are polar, their variable orientation at the interface introduces a variable dipole moment that can influence the charge injection barrier.

To test this hypothesis, we calculated the z-component of the dipole moment surface density ρ_{D_z} for the chemical modifier in each AIMD snapshot using the method described in Sec. II. In Figs. 4(a) and 4(b), we plot the electron injection barrier ϕ_e against ρ_{D_z} for the 1000 symmetrized Al/PE snapshots and 500 composite Al/PP snapshots, respectively, for each of the interface chemistries studied in this work.

Figure 4 shows a striking linear correlation between the electron injection barrier ϕ_e and the surface dipole density ρ_{D_z} for both Al/PE and Al/PP. As ρ_{D_z} increases, ϕ_e decreases. The linear relationship also reveals that the different distributions of injection barriers in Fig. 3 for interfaces with different chemical modifiers result from the distributions of ρ_{D_z} of the chemical modifiers as a result of their thermal motion.

For example, in both Al/PE and Al/PP, –CH₂Cl has a much smaller spread of ρ_{D_z} than the oxygen-containing groups due to the fact that the chlorine atom has a greater mass than the oxygen atom and is less mobile in the AIMD simulation. This, in turn, results in a smaller spread in injection barriers. As another example, a striking difference between Al/PE and Al/PP interfaces is the effect of –CH₂OH modifiers. In Al/PE, these exhibit a very large spread of ρ_{D_z}, hence resulting in a large spread of injection barriers, whereas in Al/PP, –CH₂OH modifiers show variations in ρ_{D_z} and ϕ_e that are broadly similar to –CH₂Cl. This is due to the fact that, in the AIMD simulations, –CH₂OH exhibits less orientational variation at the Al/PP interface than at the Al/PE interface. This is due to the fact that in Al/PP, the oxygen atom of –CH₂OH is closer to the Al surface than in Al/PE and, therefore, interacts with Al more strongly, which restricts the orientational variation of –CH₂OH. Our final observation is that, for the pristine interface snapshots, denoted by gray data points in each panel, ρ_{D_z} for the terminating –CH₃ chain ends is close to zero and has a very narrow distribution of values. This is expected given that –CH₃ is non-polar. Nevertheless, there is still a spread of values of ϕ_e for these pristine snapshots. Indeed, this is also the case for the snapshots with chemical modifiers: in each case, for a given value of ρ_{D_z}, there is a spread of values of ϕ_e. Our detailed investigations
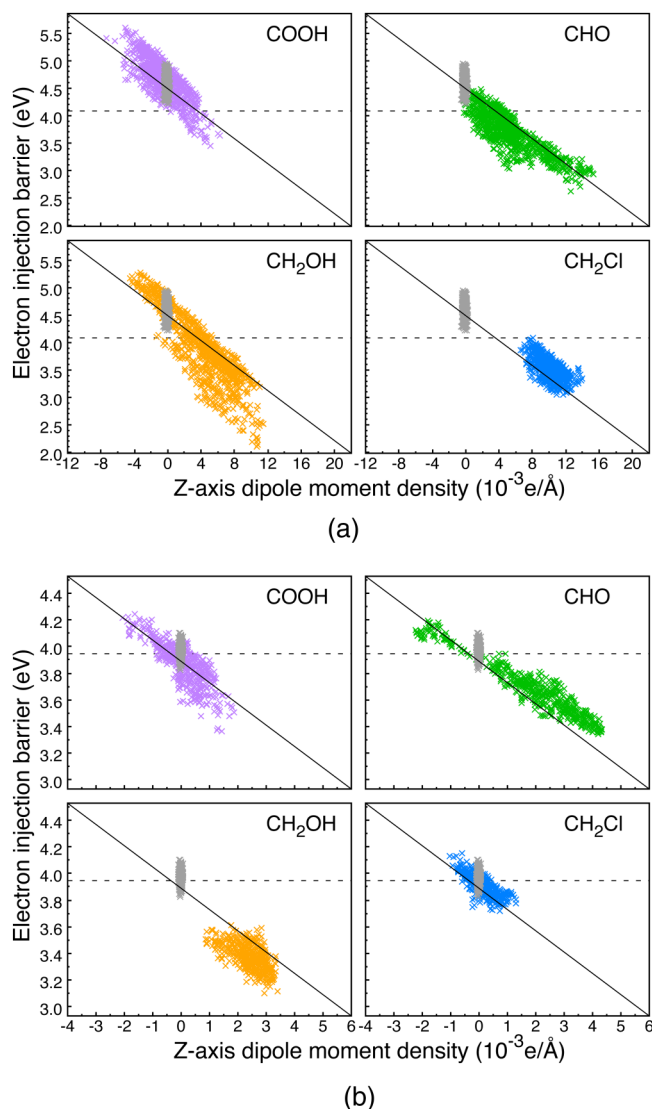
FIG. 4. The electron injection barrier ϕ_e as a function of the z-component of the surface dipole density ρ_{D_z} due to chemical modification for (a) 1000 symmetrized Al/PE snapshots and (b) 500 composite Al/PP snapshots with different chemical groups. The surface density of functional groups is "1/2" for Al/PE and "1/4" for Al/PP. The diagonal line in each panel is a linear fit to the combined data for all chemical groups for each of Al/PE and Al/PP. For comparison, the results for pristine interfaces (i.e., –CH$_3$ as the terminal group) are shown in gray in each panel. The black dashed line corresponds to $\phi_e = \phi_h$. (a) Al/PE interface. (b) Al/PP interface.

show that this spread results directly from the variation in the smallest distance between the chain end and the Al surface; in other words, it is a proximity effect.

For both Al/PE and Al/PP, we perform a linear fit to the combined data for all the chemical groups, which is shown as the diagonal black line in each panel of Fig. 4. As can be seen, the data in

each individual panel follow well the combined linear regression line, which suggests that this is a broadly universal trend that is largely independent of the specific chemistry of the modifier but rather determined primarily by the dipole moment density of the modifier. The slopes of the linear fits for Al/PE and Al/PP are similar, suggesting that there is also a strong degree of independence from the specific identity of the polymer at the interface.

A. The role of surface dipole density

Overall, our results above show that changes in charge injection barriers among snapshots are strongly determined by chemical modifiers at the interface through their surface dipole density. This observation is consistent with classical electrostatics: from the Poisson equation, it can be shown[25] that the macroscopic average potential in the interface simulation cell satisfies

$$\Delta \widehat{V} = 4\pi \widehat{p}, \tag{10}$$

where $\Delta \widehat{V}$ is the macroscopic average potential difference across the interface and $\widehat{p}$ is the macroscopic average dipole moment density at the interface. An important contribution to $\widehat{p}$ is the dipole moment surface density due to the chemical modifier, ρ_{D_z}, in Eq. (9). In other words, a change in ρ_{D_z} translates into a change in the potential difference across the interface, which results in a change in the charge injection barrier through Eqs. (6)–(8), and the relationships between these quantities are linear.

We explore this systematically by investigating how the surface density of chemical modifiers at the interface influences charge injection barriers. For each chemistry, three representative symmetrized Al/PE snapshots and composite Al/PP snapshots were chosen with z-component dipole moments ρ_{D_z} that spanned the full range of dipole moments exhibited among all the snapshots for that particular chemistry. For Al/PE, the surface densities considered were "1/2," "1/4," and "1/6," meaning that there is one chemically modified PE chain every two, four, and six chains, respectively. The interfaces with lower surface densities were constructed from the "1/2" systems by making supercells along the y-axis and retaining only one chemically modified PE chain. (Taking –COOH as an example, the numbers of atoms in the supercells of "1/2," "1/4," and "1/6" surface densities are 94, 188, and 282, respectively.) For Al/PP, we considered "1/4," "1/8," and "1/12" surface densities, with the lower surface density systems constructed from the "1/4" interfaces in a similar manner to Al/PE. Taking –COOH as an example, the numbers of atoms in the supercells of "1/4," "1/8," and "1/12" surface densities are 359, 718, and 1077, respectively.

In Fig. 5, we plot ϕ_e against ρ_{D_z} for snapshots with different representative surface densities of chemical groups for each chemical group in both Al/PE [panel (a)] and Al/PP [panel (b)]. For each chemical group, the data for each of the three chosen snapshots are represented by either circles, triangles, or squares. For a given snapshot, the value of the largest surface density is shown with a solid symbol, and the data for the other two (lower) densities are shown with an empty symbol of the same shape. In each panel, the background points in gray are the data for all the snapshots (corresponding to the largest surface density) and are equivalent to
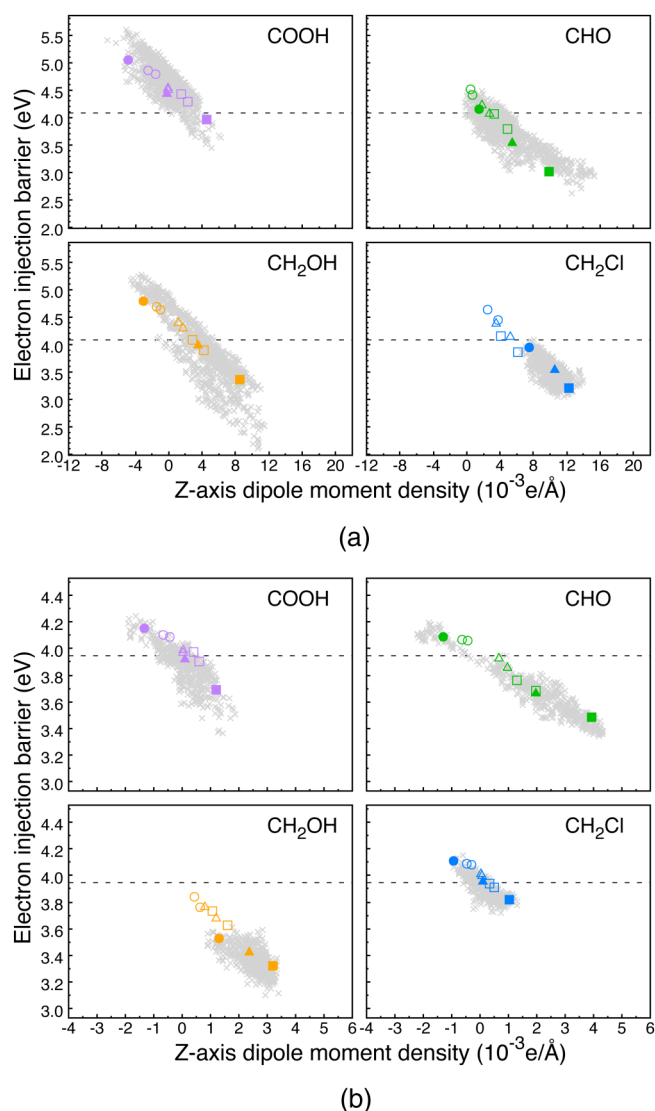
FIG. 5. The effects of surface density of chemical groups at (a) Al/PE and (b) Al/PP interfaces. For each chemical group, the data for three representative snapshots with different surface densities of the group are shown with either circles, triangles, or squares. The value for the highest surface density is shown with a solid symbol, and the data for the other surface densities are shown with empty symbols of the same shape. The background points in gray are the data of all the snapshots with the largest surface density considered. The black dashed line corresponds to $\phi_e = \phi_h$. (a) Al/PE interface. (b) Al/PP interface.

those shown in Fig. 4. The largely universal linear trend between the electron injection barrier ϕ_e and the surface dipole moment density ρ_{D_z} is again apparent, emphasizing the importance of the surface dipole moment of chemical modifiers and their thermal distribution in determining the charge injection properties of Al/PE and Al/PP interfaces.

Given the relatively small number of (large-scale) DFT calculations required for these systems (as compared to the number required to generate the data underlying Figs. 3 and 4), we sampled the Brillouin zone more densely. The k-point meshes used for symmetrized Al/PE snapshots (composite Al/PP snapshots) were $8 \times 16 \times 1$ ($6 \times 2 \times 1$), $8 \times 8 \times 1$ ($3 \times 2 \times 1$), and $8 \times 6 \times 1$ ($2 \times 2 \times 1$) for snapshots with "1/2" ("1/4"), "1/4" ("1/8"), and "1/6" ("1/12") surface densities, respectively.

IV. SUMMARY

In this paper, we have studied how the introduction of four different chemical modifiers (–COOH, –CH₂OH, –CHO and –CH₂Cl) at the chain ends of PE and PP oligomers at Al/PE and Al/PP interfaces affects electron and hole injection barriers at these interfaces. Our calculations were based on first-principles density-functional theory, and crucially, we accounted for the effect of thermal fluctuations by conducting large-scale finite-temperature *ab initio* molecular dynamics simulations to sample the range of structural conformations that Al/PE and Al/PP interfaces adopt at a temperature of around 373 K. By taking snapshots of the atomic structure of the interfaces from the AIMD trajectories, for each chemistry, we obtained an ensemble of 1000 (500) interfaces for Al/PE (Al/PP) and calculated the associated distribution of charge injection barriers. For both Al/PE and Al/PP, we found that the chemical modification can change the mean charge injection barrier by up to 1.1 and 0.6 eV for Al/PE and Al/PP, respectively, as compared to pristine interfaces without chemical modification. In terms of the spread of injection barrier values as a result of thermal fluctuations, pristine interfaces (0.14 eV for Al/PE and 0.05 eV for Al/PP) and those with –CH₂Cl (0.18 eV for Al/PE and 0.08 eV for Al/PP) have the smallest standard deviation. For Al/PE, the largest spread is found for –CH₂OH (0.61 eV), while for Al/PP, it is for –CHO (0.20 eV).

Furthermore, we have shown that these results and trends can be understood with a simple model that is based on thermal fluctuations of the dipole moment density associated with the chemical modifier at the interface. We further verify this model by considering supercells of our interface systems with lower interface surface densities of modifiers and, hence, lower surface dipole moment densities.

While our atomistic models do not exhibit the full complexity of Al/polyolefin interfaces in real devices, our work demonstrates the importance of considering the detailed atomic structure and thermal fluctuations at Al/PE and Al/PP interfaces when computing charge injection barriers. We have shown that incorporating chemical modifiers at the interface, such as those that might arise from oxidation, for example, can change charge injection barriers significantly as compared to pristine interfaces.

AUTHOR DECLARATIONS

Conflict of Interest

The authors have no conflicts to disclose.

Author Contributions

Yiyuan Wang: Data curation (equal); Formal analysis (equal); Investigation (equal); Software (equal); Visualization (equal); Writing – original draft (equal). **Sari J. Laihonen:** Formal analysis (equal); Funding acquisition (equal); Supervision (equal); Writing – review & editing (equal). **Mikael Unge:** Conceptualization (equal); Formal analysis (equal); Funding acquisition (equal); Supervision (equal); Writing – review & editing (supporting). **Arash A. Mostofi:** Conceptualization (equal); Formal analysis (equal); Funding acquisition (equal); Resources (lead); Supervision (equal); Writing – review & editing (lead).

DATA AVAILABILITY

The data that support the findings of this study are openly available in figshare at https://doi.org/10.6084/m9.figshare.23545193.v1, Ref. 41.

REFERENCES

[1]T. L. Hanley, R. P. Burford, R. J. Fleming, and K. W. Barber, IEEE Electr. Insul. Mag. **19**, 13 (2003).

[2]Y. Zhou, S. Peng, J. Hu, and J. He, IEEE Trans. Dielectr. Electr. Insul. **24**, 1308 (2017).

[3]M. Ritamäki, I. Rytöluoto, and K. Lahti, IEEE Trans. Dielectr. Electr. Insul. **26**, 1229 (2019).

[4]O. G. Gnonhoue, A. Velazquez-Salazar, É. David, and I. Preda, Polymers **13**, 766 (2021).

[5]G. Teyssedre, S. Li, K. Makasheva, N. Zhao, L. Milliere, and C. Laurent, IEEE Trans. Dielectr. Electr. Insul. **24**, 1319 (2017).

[6]T. D. Huan, S. Boggs, G. Teyssedre, C. Laurent, M. Cakmak, S. Kumar, and R. Ramprasad, Prog. Mater. Sci. **83**, 236 (2016).

[7]L. Chen, T. D. Huan, and R. Ramprasad, Sci. Rep. **7**, 6128 (2017).

[8]G. Teyssedre, F. Zheng, L. Boudou, and C. Laurent, J. Phys. D: Appl. Phys. **54**, 26 (2021).

[9]G. Chen, M. Hao, Z. Xu, A. Vaughan, J. Cao, and H. Wang, CSEE J. Power Energy Syst. **1**, 9 (2015).

[10]G. Teyssedre, C. Laurent, A. Campus, U. Nilsson, and G. Montanari, in *2003 Annual Report Conference on Electrical Insulation and Dielectric Phenomena* (IEEE, 2003), pp. 96–99.

[11]S. Guimond, I. Radu, G. Czeremuszkin, D. J. Carlsson, and M. R. Wertheimer, Plasmas Polym. **7**, 71 (2002).

[12]N. Bhat and D. Upadhyay, J. Appl. Polym. Sci. **86**, 925 (2002).

[13]S. Mirabedini, H. Arabi, A. Salem, and S. Asiaban, Prog. Org. Coat. **60**, 105 (2007).

[14]J. Friedrich, *The Plasma Chemistry of Polymer Surfaces: Advanced Techniques for Surface Design* (John Wiley & Sons, 2012).

[15]C. Laurent, G. Teyssedre, S. Le Roy, and F. Baudoin, IEEE Trans. Dielectr. Electr. Insul. **20**, 357 (2013).

[16]M. Taleb, G. Teyssedre, S. Le Roy, and C. Laurent, IEEE Trans. Dielectr. Electr. Insul. **20**, 311 (2013).

[17]M. Q. Hoang, M. Q. Nguyen, T. T. N. Vu, G. Teyssedre, and S. Le Roy, J. Phys. D: Appl. Phys. **54**, 305303 (2021).

[18]E. Doedens, E. M. Jarvid, R. Guffond, and Y. V. Serdyuk, Energies **13**, 1750 (2020).

[19]L. Chen, T. D. Huan, Y. C. Quintero, and R. Ramprasad, J. Mater. Sci. **51**, 506 (2016).

[20]A. Huzayyin, S. Boggs, and R. Ramprasad, in *2011 Annual Report Conference on Electrical Insulation and Dielectric Phenomena* (IEEE, 2011), pp. 800–803.

[21]M. El-Shahat, A. Huzayyin, and H. Anis, IEEE Trans. Dielectr. Electr. Insul. **26**, 642 (2019).

[22]G. Stevens, A. Pye, A. Vaughan, C. Green, and J. Pilgrim, in *2016 IEEE International Conference on Dielectrics (ICD)* (IEEE, 2016), Vol. 1, pp. 272–275.

[23]J. S. Ho and S. G. Greenbaum, ACS Appl. Mater. Interfaces **10**, 29189 (2018).

[24]C. G. Van de Walle and R. M. Martin, Phys. Rev. B **35**, 8154 (1987).

[25]J. Junquera, M. H. Cohen, and K. M. Rabe, J. Phys.: Condens. Matter **19**, 213203 (2007).

[26]P. Giannozzi, O. Andreussi, T. Brumme, O. Bunau, M. B. Nardelli, M. Calandra, R. Car, C. Cavazzoni, D. Ceresoli, M. Cococcioni, N. Colonna, I. Carnimeo, A. D. Corso, S. de Gironcoli, P. Delugas, R. A. DiStasio, Jr., A. Ferretti, A. Floris, G. Fratesi, G. Fugallo, R. Gebauer, U. Gerstmann, F. Giustino, T. Gorni, J. Jia, M. Kawamura, H.-Y. Ko, A. Kokalj, E. Küçükbenli, M. Lazzeri, M. Marsili, N. Marzari, F. Mauri, N. L. Nguyen, H.-V. Nguyen, A. O. de-la Roza, L. Paulatto, S. Poncé, D. Rocca, R. Sabatini, B. Santra, M. Schlipf, A. P. Seitsonen, A. Smogunov, I. Timrov, T. Thonhauser, P. Umari, N. Vast, X. Wu, and S. Baroni, J. Phys.: Condens. Matter **29**, 465901 (2017).

[27]J. P. Perdew, K. Burke, and M. Ernzerhof, Phys. Rev. Lett. **77**, 3865 (1996).

[28]A. M. Rappe, K. M. Rabe, E. Kaxiras, and J. Joannopoulos, Phys. Rev. B **41**, 1227 (1990).

[29]C. Kittel and P. McEuen, *Introduction to Solid State Physics* (Wiley, New York, 1976), Vol. 8.

[30]T. Thonhauser, S. Zuluaga, C. Arter, K. Berland, E. Schröder, and P. Hyldgaard, Phys. Rev. Lett. **115**, 136402 (2015).

[31]T. Thonhauser, V. R. Cooper, S. Li, A. Puzder, P. Hyldgaard, and D. C. Langreth, Phys. Rev. B **76**, 125112 (2007).

[32]K. Berland, V. R. Cooper, K. Lee, E. Schröder, T. Thonhauser, P. Hyldgaard, and B. I. Lundqvist, Rep. Prog. Phys. **78**, 066501 (2015).

[33]D. Langreth, B. I. Lundqvist, S. D. Chakarova-Käck, V. Cooper, M. Dion, P. Hyldgaard, A. Kelkkanen, J. Kleis, L. Kong, S. Li *et al.*, J. Phys.: Condens. Matter **21**, 084203 (2009).

[34]G. Avitabile, R. Napolitano, B. Pirozzi, K. Rouse, M. Thomas, and B. Willis, J. Polym. Sci.: Polym. Lett. Ed. **13**, 351 (1975).

[35]G. Natta and P. Corradini, Il Nuovo Cimento **15**, 40 (1960).

[36]K. Less and E. Wilson, J. Phys. C: Solid State Phys. **6**, 3110 (1973).

[37]H. Xie, X. Wu, Z. Peng, and H. Zhang, in *Proceedings of 1994 4th International Conference on Properties and Applications of Dielectric Materials (ICPADM)* (IEEE, 1994), Vol. 1, pp. 39–41.

[38]J. P. Perdew, M. Ernzerhof, and K. Burke, J. Chem. Phys. **105**, 9982 (1996).

[39]A. Moyassari, M. Unge, M. S. Hedenqvist, U. W. Gedde, and F. Nilsson, J. Chem. Phys. **146**, 204901 (2017).

[40]S. Le Roy, G. Teyssedre, C. Laurent, G. Montanari, and F. Palmieri, J. Phys. D: Appl. Phys. **39**, 1427 (2006).

[41]Y. Wang (2023). Data for calculations. figshare. https://doi.org/10.6084/m9.figshare.23545193.v1.

26 September 2023 13:26:46